

Flow and mass transfer around a core-shell reservoir

Badr Kaoui*

*Biomechanics and Bioengineering Laboratory UMR 7338, CNRS, Sorbonne University,
University of Technology of Compiègne, 60200 Compiègne, France*

(Received 22 February 2017; published 15 June 2017)

I have developed an alternative numerical approach to study mass transfer from a stationary core-shell reservoir under channel flow conditions. I use the lattice Boltzmann method to compute both the solvent fluid flow and the diffusion and advection of the solute. I have investigated the impact of the flow by reporting mass transfer quantities such as the instantaneous solute concentration and the local Sherwood number at the surface of the reservoir. The flow is found to enhance the release of the encapsulated material, but it prevents the released material from reaching the channel walls.

DOI: [10.1103/PhysRevE.95.063310](https://doi.org/10.1103/PhysRevE.95.063310)**I. PROBLEM STATEMENT**

Understanding mass transfer under flow conditions is of fundamental and practical interest. Many natural phenomena and industrial processes involve the diffusion, advection, and reaction of chemical substances (solutes) and the flow of their surrounding fluid (solvent). In the present study, I am rather interested in the release of a substance from a reservoir under flow conditions. The reservoir is made of an inner core medium (fluid or solid) coated with an outer shell. The substance is initially loaded into the core and it is protected from the external environment by the shell. The release of the substance from the core is controlled by the shell. This study is initially motivated to gain insight into the fundamentals of mutual coupling between three components: fluid flow, structure, and mass transfer. Direct applications can be found in the newly flourishing discipline of controlled release systems, such as targeted drug delivery systems [1]: core-shell capsules [2] or core-shell fibers [3].

Few studies in the literature have dealt with the problem of release from a core-shell reservoir and most of them have considered no flow conditions [4,5], for simplification reasons. For such a situation, the release is mainly controlled by the shell properties, such as its thickness and permeability, and there are even some empirical laws that give the release rate [4]. However, the presence of an external applied flow (forced convection) increases the complexity of the problem. While there is no systematic study on release from core-shell reservoir under flow, many other studies have considered mass transfer from particles (including drops and bubbles) under flow [6]. At low Péclet number (a dimensionless number that measures the importance of advection with respect to diffusion), the problem can be even solved analytically. However, most of these studies have assumed uniform and constant boundary conditions at the particle surface, as also pointed out recently in Ref. [7], and do not match my actual problem.

Here I consider release from a single isolated core-shell reservoir particle under flow with unsteady mass transfer boundary conditions at the shell. I study the distribution of the released substance (solute) as a function of the Péclet number

for a given flow pattern, here laminar, steady, and symmetric around the particle. I consider the shell as a porous membrane, which allows transport of the solute, but not the solvent. It is impermeable to the external fluid. This simplifies the problem by avoiding the swelling and deflation of the reservoir. I solve the problem in two-dimensional (2D) space. This reduction in the problem dimensionality would not alter the physics of the system. The system in two dimensions would correspond to the case of a cylindrical core-shell reservoir that is extended to infinity in the third dimension. This corresponds to either the 2D version of a spherical capsule [2] or the 3D case of a fiber [3]. Anyway, no direct quantitative comparison with fully 3D experimental data is planned at this stage of the work. I am rather interested in investigating the qualitative behavior. The core medium is initially loaded with a high concentration of the solute. This establishes a concentration gradient at the two sides of the shell and triggers the pure diffusion of the solute from the core, through the shell into the ambient fluid, in other words, the release of the reservoir content into the external medium. The system is at an out-of-equilibrium state at the beginning and tends to relax towards an equilibrium state until exhaustion of the encapsulated material.

I consider a steady nonmoving obstacle in order to remove the effect of a moving reservoir on the flow and thus on the mass transfer. The reservoir is kept stationary at the centerline of the channel at a given location from the channel inlet. Such a setup is practical to measure experimentally the concentration using, for example, the fluorescence microscopy and the flow around the reservoir by the particle image velocimetry while having a nonmoving reservoir in the laboratory reference frame. This avoids tracking at the same time both the motion of the reservoir and the release of its inner substance, which is not a trivial easy task. This setup is also very close to the case of studying the problem in the particle center-of-mass reference frame while considering an externally applied uniform flow, as usually done analytically [6,7].

The article is organized as follows. In Sec. II I will introduce briefly the lattice Boltzmann method and how I set and adapt it to compute both the flow and the mass transfer around a stationary obstacle, the reservoir. In Sec. III I report how the flow alters the main physical quantities of mass transfer: the instantaneous solute concentration and the local and total Sherwood number (the dimensionless version of the mass transfer coefficient). A summary is given in Sec. IV.

*badr.kaoui@utc.fr

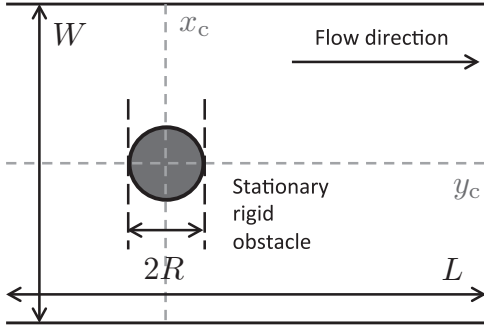


FIG. 1. Geometry of the problem for the flow part.

II. NUMERICAL METHOD

The lattice Boltzmann method (LBM) is the suitable numerical technique to solve such multiphysics problem: coupling mass transfer with fluid flow passing an obstacle in a channel. This method is well established; therefore, I will not give more details about it here. I rather refer the readers to the textbooks of Succi (for the physics basis of the LBM) [8], Sukop and Thorne (for the engineering applications of the LBM) [9], and Wolf-Gladrow (for the mathematics of the LBM) [10]. Here I give only the main steps on how I adapt and set the LBM to solve the problem by computing both the fluid flow and the mass transfer.

Flow solver. The problem involves the flow of a fluid (solvent) around a stationary rigid cylinder (as depicted in Fig. 1), which can be computed by solving the continuum Navier-Stokes equations

$$\frac{\partial \mathbf{u}}{\partial t} + \mathbf{u} \cdot \nabla \mathbf{u} = -\frac{\nabla p}{\rho} + \nu \nabla^2 \mathbf{u}, \quad \nabla \cdot \mathbf{u} = 0, \quad (1)$$

where $\mathbf{u}(x, y, t)$ and $p(x, y, t)$ are the local velocity and pressure of the fluid at the position $\mathbf{r} \equiv (x, y)$ and at time t , respectively, and ρ and ν are the mass density and the kinematic viscosity of the fluid, respectively, which are assumed to be constant and uniform throughout this study. The computational domain is divided into two domains: the fluid domain (the white area in Fig. 1) and the reservoir domain (the gray area), seen as a stationary rigid obstacle. Instead of solving Eqs. (1) using, e.g., the finite-element method or finite-volume method, I use the LBM. The main quantity of interest in the LBM is the distribution function f_i that gives the probability to find a population of fluid particles at the discrete position (x, y) with the i th discrete velocity vector \mathbf{e}_i , with $i = 0-8$ for the D2Q9 lattice. The evolution of f_i is given by the lattice Boltzmann equation

$$f_i(\mathbf{r} + \mathbf{e}_i, t + 1) - f_i(\mathbf{r}, t) = -\frac{f_i(\mathbf{r}, t) - f_i^{\text{eq}}(\mathbf{r}, t)}{\tau_f}, \quad (2)$$

where

$$f_i^{\text{eq}}(\mathbf{r}, t) = \omega_i \rho \left[1 + 3(\mathbf{u} \cdot \mathbf{e}_i) + \frac{9}{2}(\mathbf{u} \cdot \mathbf{e}_i)^2 - \frac{3}{2}(\mathbf{u}^2) \right], \quad (3)$$

with the D2Q9 lattice weight factors: $\omega_i = \frac{4}{9}$ for $i = 0$; $\omega_i = \frac{1}{9}$ for $i = 1, 2, 3, 4$; and $\omega_i = \frac{1}{36}$ for $i = 5, 6, 7, 8$. Here the right-hand side of Eq. (2) expresses the Bhatnagar-Gross-Krook (BGK) relaxation scheme: f_i relaxes towards equilibrium f_i^{eq} within a microscopic characteristic time τ_f . This later is related

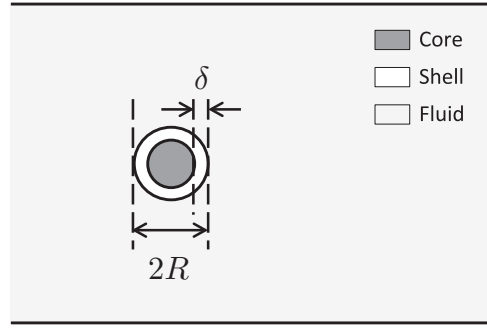


FIG. 2. Geometry of the problem for the mass transfer part.

to the macroscopic kinematic viscosity of the fluid via the formula $\nu = \frac{1}{3}(\tau_f - \frac{1}{2})$. Body forces can be included by adding a forcing term to the right-hand side of Eq. (2) as explained in Ref. [11]. The velocity can be computed then as the first moment of f_i :

$$\mathbf{u}(x, y, t) = \frac{1}{\rho} \sum_{i=0}^8 f_i(x, y, t) \mathbf{e}_i \quad \text{with} \quad \rho = \sum_{i=0}^8 f_i(x, y, t). \quad (4)$$

A flow with parabolic velocity profile having a maximum u_{max} at the channel centerline is generated by exerting a constant body force uniformly distributed in the fluid domain: $\mathbf{f}_b(x, y) = (8\rho\nu u_{\text{max}}/W, 0)$ in the x direction.

Flow boundary conditions. I set zero nonslip velocity boundary conditions along the channel walls and at the reservoir surface, via the LBM bounceback boundary condition, and I set periodic boundary conditions at the channel inlet and outlet.

Mass transfer solver. The diffusion and advection of a solute is described by the equation

$$\frac{\partial c}{\partial t} + \mathbf{u} \cdot \nabla c = D \nabla^2 c, \quad (5)$$

where $c(x, y, t)$ is the local concentration of the solute and D its diffusion coefficient. In this study, I consider one-way coupling (also known as the passive-tracer limit [12]). That means the flow alters locally the solute concentration evolution via the advection term $\mathbf{u} \cdot \nabla c$ in Eq. (5), while the concentration has no impact on either the fluid flow or its hydrodynamical properties (ν and ρ).

Again, instead of solving directly Eq. (5), I use the LBM. I use another additional distribution function $g_i(x, y, t)$ in a second lattice Boltzmann equation [similar to Eq. (2) but with g_i] to compute the diffusion and advection of the concentration

$$g_i(\mathbf{r} + \mathbf{e}_i, t + 1) - g_i(\mathbf{r}, t) = -\frac{g_i(\mathbf{r}, t) - g_i^{\text{eq}}(\mathbf{r}, t)}{\tau_d}, \quad (6)$$

where

$$g_i^{\text{eq}}(\mathbf{r}, t) = \omega_i c(\mathbf{r}, t) \left[1 + 3(\mathbf{u} \cdot \mathbf{e}_i) + \frac{9}{2}(\mathbf{u} \cdot \mathbf{e}_i)^2 - \frac{3}{2}(\mathbf{u}^2) \right]. \quad (7)$$

Here g_i^{eq} includes also the nonlinear terms and not only the linear one, as classically done (see, e.g., Refs. [9, 12]). Moreover, I let g_i exist on the same D2Q9 lattice as f_i , even though the D2Q5 lattice is sufficient for the mass transfer part. This allows performing twice the same LBM steps (streaming, collision,

etc.), however with different boundary conditions, bulk forces (source terms), and solid nodes (Figs. 1 and 2) for each of the distribution functions f_i and g_i . For the mass transfer part, the macroscopic diffusion coefficient D is related to a microscopic characteristic time τ_d [equivalent to τ_f in Eq. (2)] via $D = \frac{1}{3}(\tau_d - \frac{1}{2})$. The local concentration is given as the zeroth-order moment of g_i :

$$c(x, y, t) = \sum_{i=0}^8 g_i(x, y, t). \quad (8)$$

Mass transfer boundary conditions. The way of implementing properly the boundary conditions for diffusion, especially on curved interfaces, within the framework of the LBM is still an actual matter of development [13]. Here I get around this issue by using the same technique as used to implement the viscosity contrast [11] and the thermal conductivity contrast [14] for particles under flow. The computational domain for the mass transfer part is divided into three domains: the core, the shell, and the fluid, as depicted in Fig. 2. A different diffusion coefficient D is associated with each domain by setting a different BGK relaxation time τ_d . Thus, $D \equiv D(x, y)$ is a spatial function and it has three different values depending on whether the computation node (x, y) is located in the core, the shell, or the fluid. This simple numerical approach may seem naive, but it has demonstrated its credibility in capturing the correct physics in Refs. [11, 14–16]. This approach achieves the continuity of the concentration at the core-shell interface and at the shell-fluid interface. Moreover, with a nonzero shell thickness ($\delta \neq 0$), the unsteady mass flux across the particle surface is implemented naturally and straightforwardly. Zero mass flux is set along the channel walls via the LBM bounce-back boundary condition [9], as for the flow part, and periodic boundary conditions are set at the channel inlet and outlet.

Initial conditions. The fluid is initially at rest and flow is driven by applying the body force \mathbf{f}_b until it reaches the fully developed flow regime. For the concentration, $c(x, y, 0)$ is set to $c_0 = 10$ in the core and zero elsewhere.

Benchmark tests. The flow part of the code is benchmarked separately by recovering exactly the analytical expression of a parabolic velocity profile in the absence of an obstacle. The mass transfer part is also benchmarked separately by comparing the obtained numerical data with analytical profiles for pure diffusion in infinite domains [17]. Such benchmarking tests are reported in Ref. [9]. For both the flow and the mass transfer parts, the numerical data match exactly the analytical solutions when the relaxation time parameters (τ_f and τ_d) are taken within the range $]0.5, 2]$, which is used in all the simulations below. There is no validation test for the problem of the release from a core-shell reservoir immersed in a channel and subjected to flow.

Key physical parameters. The results are given as a function of the control dimensionless numbers: the Reynolds number

$$\text{Re} = \frac{u_{\max} R}{\nu}, \quad (9)$$

which measures the importance of inertia and is taken to be unity in all the simulations, and the Péclet number

$$\text{Pe} = \frac{u_{\max} R}{D}, \quad (10)$$

which gives the importance between the advection and the diffusion. It will be varied by varying only D in order to keep the same $\text{Re} = 1$ and thus the same flow pattern. The Schmidt number

$$\text{Sc} = \frac{\nu}{D} \quad (11)$$

relates the Reynolds number to the Péclet number via the expression $\text{Pe} = \text{Re Sc}$. Here $\text{Sc} = \text{Pe}$ since $\text{Re} = 1$. There is also the blockage ratio number $B = 2R/W$ that controls the transition to different regimes of flow passing an obstacle in a channel. It is held constant. Time is expressed in dimensionless form using the Fourier number $\text{Fo} = Dt/R^2$.

III. RESULTS AND DISCUSSION

All the results reported below are obtained with a Reynolds number set to unity $\text{Re} = 1$ and $B = 0.225$. The computational domain is set to $L = 1600$ and $W = 400$. All the reservoir geometrical parameters are kept the same for all the simulations: The reservoir radius $R = 45$ with a shell thickness $\delta = 15$. The obtained flow is then steady and laminar and does not exhibit any recirculation wake patterns at the rear of the reservoir. The Péclet number is varied while keeping the Reynolds number constant. The other parameters are in lattice units: $u_{\max} = 0.037$, $\tau_f = 1$, $\rho\nu = 1/6$, $\tau_d(\text{core}) = 1$, $\tau_d(\text{shell}) = 0.55$, and $\tau_d(\text{fluid}) = 0.9995, 0.5999, 0.54995, 0.51998, 0.50999$ for $\text{Pe} = 10, 50, 100, 250, 500$, respectively.

Developing fluid flow case. Figure 3 shows the evolution in time of the velocity field (the gray vectors) and the concentration (the color map) for $\text{Pe} = 50$. Due to the diffusion across the shell, the solute escapes from the core reservoir into the ambient fluid. At the early stage, when the flow is still weak, the mass transfer is dominated by diffusion and the concentration boundary layer is almost radially symmetric with respect to the reservoir center of mass (x_c, y_c) . Later on the flow develops into steady and laminar flow that pushes the concentration boundary layer downstream behind the reservoir. The snapshots are taken at equal time intervals. The range of the color bar box varies from one snapshot to another. Its upper limit decreases with time because the local concentration tends everywhere towards a lower equilibrium value. At a later stage, the fluid reaches a fully developed flow regime. The flow has a parabolic velocity profile far from the reservoir location, in the vicinity of the channel inlet and outlet. The same figure shows the distribution of the solute concentration in the same computational domain. Later on the concentration boundary layer is gradually punched off in the flow direction. The flow prevents the solute from reaching the channel walls. However, behind the reservoir the flow recovers its parabolic shape. It slows down and the diffusion regains control and thus the concentration spreads until it reaches the channel walls.

To appreciate more the distribution of the solute, I report in Fig. 4 the concentration profiles taken along the reservoir center of mass location x_c and at different moments. Figure 4(a) shows the concentration profiles for the stagnant fluid case and Fig. 4(b) for the flowing fluid case. The gray colored areas indicate the location of the shell. The concentration in the core decreases with time, it gets a slope along the shell, and it decays in the fluid. The solute leakage is accelerated in the presence of

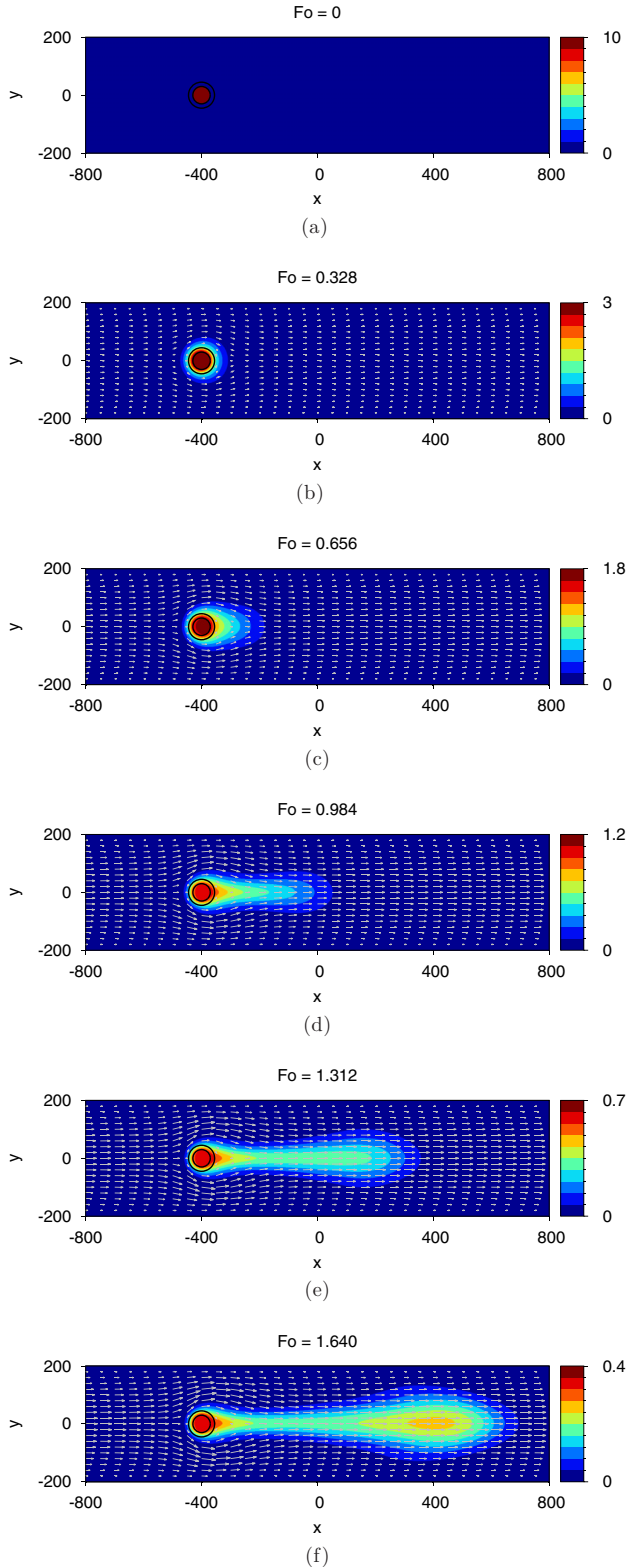


FIG. 3. Evolution of flow and mass transfer around a stationary rigid core-shell reservoir. The fluid is initially at rest and it develops into a laminar steady flow. The core is initially loaded with a high concentration $c_0 = 10$ that creates a gradient with the rest of the domain, where the solute is initially absent. The concentration gradient triggers the release, from the core into the ambient fluid, until exhaustion of the internal solute and until it reaches equilibrium. Snapshots are taken at equal time intervals. Here $Pe = 50$.

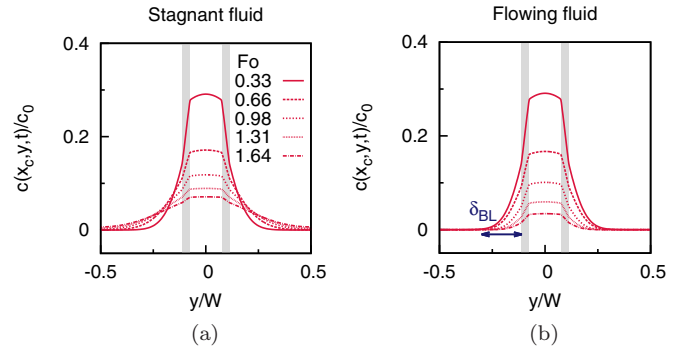


FIG. 4. Solute concentration profiles taken along the line $x = x_c$ at different moments, for (a) stagnant fluid and (b) flowing fluid. The gray areas indicate the location of the shell. Under flow conditions, the released solute stays in the vicinity of the reservoir surface and the thickness of the boundary layer δ_{BL} stays roughly constant.

the flow. The height of the profiles at a later stage is lower for the stagnant fluid case. So the flow enhances the release of the encapsulated material into the ambient flowing fluid. However, the released material stays close to the reservoir surface and it does not diffuse laterally towards the channel walls. It builds up a concentration boundary layer, for which the thickness δ_{BL} stays roughly constant. For the stagnant fluid case, δ_{BL} extends with time and the released material diffuses radially until it reaches the channel walls.

Impact of the Péclet number. The data obtained for different values of the Péclet number Pe are reported in Fig. 5. These data are taken when the core has released 80% of its initial loaded material. Here the simulations are performed by setting initially a fully developed flow, obtained with $Re = 1$, similar to the one reported in Fig. 3(f). Fully developed flow allows appreciating the effect of Pe for the same flow pattern, while ruling out the transient regime effects. For all nonzero Pe , the flow restricts the released solute within the vicinity of the reservoir surface and extends its concentration boundary layer downstream behind the reservoir. This boundary layer shrinks more around the reservoir and extends further into the flow direction when increasing Pe . Thus, the flow breaks the radial symmetry of the diffusion front [Fig. 5(a)] and alters also the solute concentration distribution within the shell and the core.

Flow impact on mass transfer quantities. The impact of flow (fully developed flow case) can be well described by reporting the mass transfer physical quantities on the surface of the reservoir. Figure 6 gives the instantaneous local surface concentration $c(R, \theta, t)$, the instantaneous local mass flux $J(\theta, t)$, and the instantaneous local Sherwood number $Sh(\theta, t)$, defined as

$$J(\theta, t) = -D \left[\frac{c(R, \theta, t) - c(R - \delta, \theta, t)}{\delta} \right], \quad (12)$$

$$h(\theta, t) = -\frac{D}{c(R, \theta, t)} \left[\frac{\partial c}{\partial r} \right]_{r=R}, \quad (13)$$

$$Sh(\theta, t) = 2 \frac{R}{D} h(\theta, t), \quad (14)$$

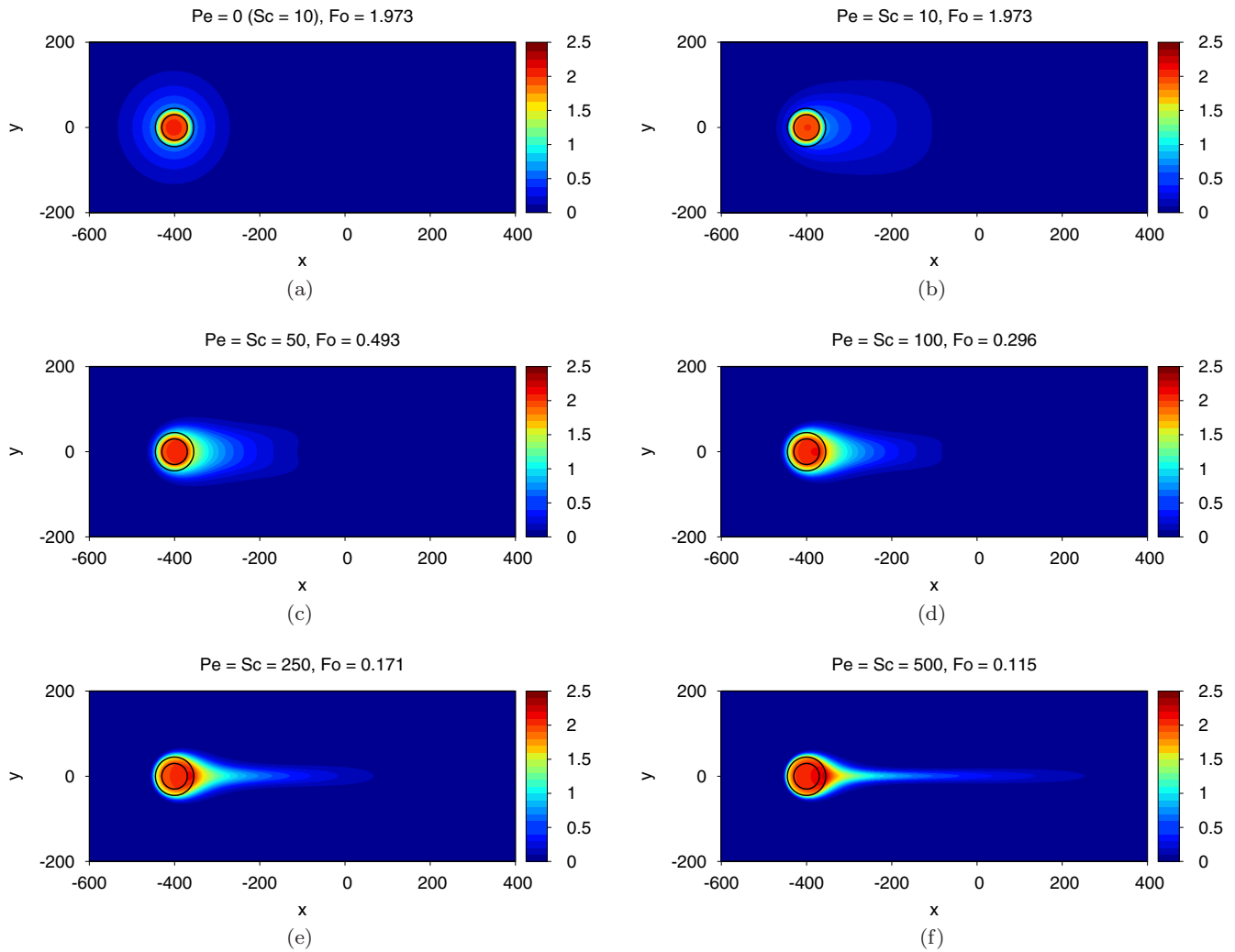


FIG. 5. Distribution of the solute as a function of the Péclet number Pe , for the same fully developed flow pattern around the reservoir, when 80% of the initially encapsulated amount is released. Here Pe is increased by decreasing the value of the diffusion coefficient in the fluid D while holding all the other parameters constant. The concentration boundary layer gets thinner and extends farther downstream when increasing Pe .

where θ is the angular position as defined in Fig. 6(a). The Sherwood number $Sh(\theta, t)$ is the dimensionless version of the mass transfer coefficient $h(\theta, t)$ and it is equivalent to the Nusselt number used for heat transfer. Equation (12) is evaluated using the diffusion coefficient in the shell, while

Eqs. (13) and (14) are evaluated with the diffusion coefficient in the ambient fluid. Figure 6(b) shows that the solute concentration at the surface of the reservoir is not uniform, in contrast to the stagnant fluid case in which it is uniform. It is lower in front of the reservoir and higher behind it. Moreover,

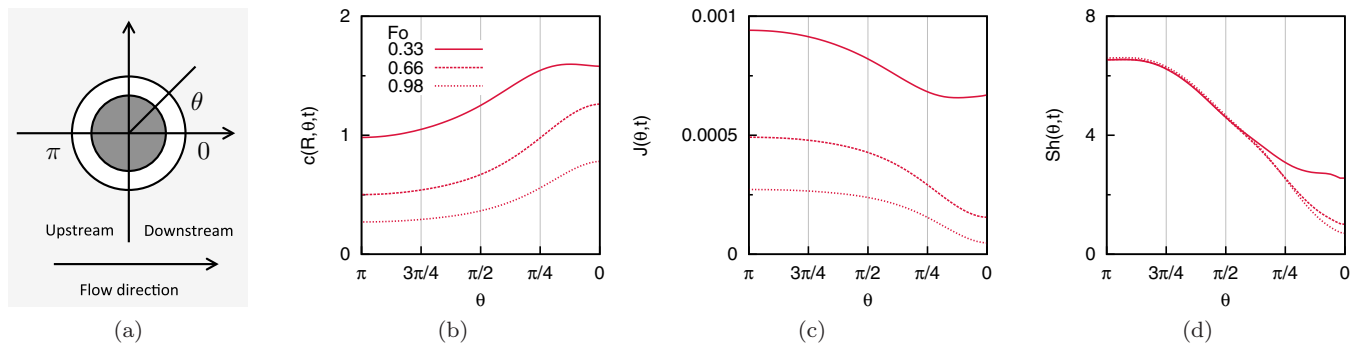


FIG. 6. (a) Angular position θ , (b) instantaneous solute concentration at the surface of the reservoir $c(R, \theta, t)$, (c) instantaneous local mass flux across the shell $J(\theta, t)$, and (d) instantaneous local Sherwood number $Sh(\theta, t)$, taken at three different moments. All these quantities are not constant and are not uniform at the surface of the reservoir.

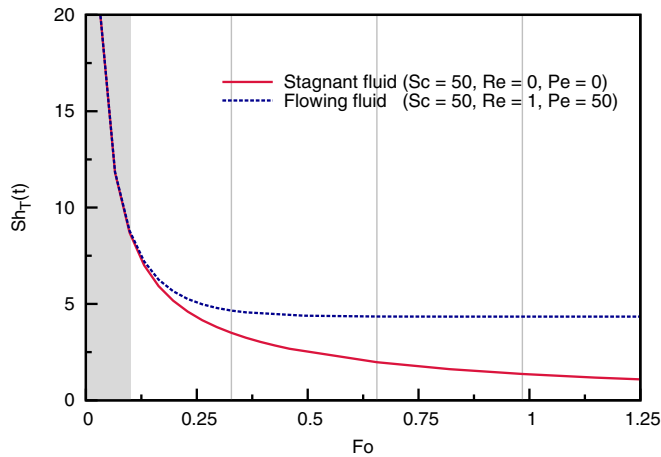


FIG. 7. Instantaneous total Sherwood number $Sh_T(t)$ for a stagnant fluid (solid red line) and for a flowing fluid with Péclet number $Pe = 50$ (dashed blue line). The overall mass transfer from the core-shell reservoir is enhanced by the flow.

the concentration at the surface is not constant, but it evolves in time due to the established unsteady mass flux across the shell. In most previous studies on mass transfer from particles, the concentration is assumed to be uniform and constant at the particle surface [6]. Here the system is placed at an out-of-equilibrium state by setting initially a concentration gradient on both sides of the shell and that triggers the diffusion. Thus, relaxation towards an equilibrium state. The generated mass flux is important upstream at the front of the reservoir and is less downstream, as shown in Fig. 6(c). The flux is higher upstream because the flow washes away downstream the newly released material. This creates a lower surface concentration that results in a high-concentration gradient with the internal slowly evolving concentration. The local Sherwood number as a function of the angle is shown in Fig. 6(d). It is higher upstream and lower downstream. Its value is not also constant and uniform. It is different from the classical constant and uniform value $Sh = 2$ computed for a particle with constant boundary conditions on its surface and subjected to unbounded uniform Stokes flow [6]. In both Figs. 6(b) and 6(c) $c(R, \theta, t)$ and $J(\theta, t)$ exhibit noticeable evolution in time, while $Sh(\theta, t)$ only weakly evolves with time [Fig. 6(d)].

Total Sherwood number. Figure 7 shows the instantaneous total Sherwood number for a stagnant fluid (solid red line) and for a flowing fluid (dashed blue line), which corresponds to Péclet numbers $Pe = 0$ and $Pe = 50$, respectively. I report data obtained before the concentration boundary layer reaches the channel outlet boundary. The total Sherwood number $Sh_T(t)$ is obtained by integrating the local Sherwood number $Sh(\theta, t)$ over the surface of the reservoir (here in two dimensions over its circumference): $Sh_T(t) = \frac{1}{2\pi R} \int_{\theta=0}^{2\pi} Sh(\theta, t) ds(\theta)$. Higher and exactly identical values of the Sherwood number are

measured at the early stage of the simulations for both cases (the gray area). At this stage, the flow has no effect on the mass transfer, even though the flow is already fully developed. The mass transfer is taking place mainly by pure diffusion. The amount of the released solute around the reservoir is still negligible for advection to play a part. Later on the two curves detach. The Sherwood number for the stagnant fluid case decreases rapidly and tends to vanish. For this pure diffusion scenario, the mass transfer rate (the mass flux) drops gradually in time and tends to vanish at equilibrium (when the concentrations at both sides of the shell reach an equal equilibrium value), while the one for the flowing fluid plateaus around $Sh_T = 5$, which is higher. Due to advection, the solute is washed away each time from the reservoir surface, causing the external concentration to drop down [Fig. 6(b)]. Thus, the concentration gradient drops slowly and so does the mass transfer coefficient. For the flowing fluid case, the flow creates a concentration boundary layer with a thickness that is maintained constant enough in time. This is why the Sherwood number plateaus momentarily for the flowing fluid case until exhaustion of the encapsulated material. The flow enhances the overall mass transfer from the core-shell reservoir.

IV. CONCLUSION

I have adapted the lattice Boltzmann method to couple and compute both the flow and mass transfer around a core-shell reservoir. For the boundary conditions, I have used a simple algorithm that allows having the mass transfer in a heterogeneous medium with curved interfaces and allows implementing unsteady jump boundary conditions on these interfaces.

I have presented results of the LBM simulations showing the released solute distribution under flow condition and report how the flow affects the mass transfer quantities such as the concentration of the solute at the reservoir surface, the local mass flux across the shell, and the local Sherwood number. All the simulations imply nonuniform unsteady mass transfer boundary condition at the reservoir surface, in contrast to the classical studies. The flow is found to enhance the solute release from the core-shell reservoir. However, it hinders the spread of the released solute to the channel walls. Such qualitative and quantitative data are not available in literature, especially for the core-shell reservoir system, despite their relevance, for example, to the fields of chemical engineering and pharmaceuticals.

ACKNOWLEDGMENT

Most of the simulations have been performed on the Plateforme Inter-Laboratoire de Calcul et de Modélisation Multidisciplinaire PILCAM2 of the University of Technology of Compiègne.

[1] M. W. Tibbitt, J. E. Dahman, and R. Langer, Emerging frontiers in drug delivery, *J. Am. Chem. Soc.* **138**, 704 (2016).

[2] S. Seiffert, J. Thiele, A. R. Abate, and D. A. Weitz, Smart microgel capsules from macromolecular precursors, *J. Am. Chem. Soc.* **132**, 6606 (2010).

- [3] L. Romano, A. Camposeo, R. Manco, M. Moffa, and D. Pisignano, Core-shell electrospun fibers encapsulating chromophores or luminescent proteins for microscopically controlled molecular release, *Mol. Pharm.* **13**, 729 (2016).
- [4] R. W. Baker, *Controlled Release of Biologically Active Agents* (Wiley, New York, 1987).
- [5] D. Morvan and M. Y. Jaffrin, Unsteady diffusion mass transfer in a microencapsulated islet of Langerhans for a bioartificial pancreas, *Int. J. Heat Mass Transfer* **32**, 995 (1989).
- [6] R. Clift, J. R. Grace, and M. E. Weber, *Bubbles, Drops, and Particles* (Academic Press, New York, 1978).
- [7] V. Vandadi, S. Jafari Kang, and H. Masoud, Reciprocal theorem for convective heat and mass transfer from a particle in Stokes and potential flows, *Phys. Rev. Fluids* **1**, 022001(R) (2016).
- [8] S. Succi, *The Lattice Boltzmann Equation for Fluid Dynamics and Beyond* (Oxford University Press, Oxford, 2001).
- [9] M. C. Sukop and D. T. Thorne, *Lattice Boltzmann Modeling* (Springer, Berlin, 2006).
- [10] D. A. Wolf-Gladrow, *Lattice-Gas Cellular Automata and Lattice Boltzmann Models: An Introduction* (Springer, Berlin, 2000).
- [11] B. Kaoui and J. Harting, Two-dimensional lattice Boltzmann simulations of vesicles with viscosity contrast, *Rheol. Acta* **55**, 465 (2016).
- [12] S. G. Ayodele, F. Varnik, and D. Raabe, Effect of aspect ratio on transverse diffusive broadening: A lattice Boltzmann study, *Phys. Rev. E* **80**, 016304 (2009).
- [13] K. Guo, L. Li, G. Xiao, N. AuYeung, and R. Mei, Lattice Boltzmann method for conjugate heat and mass transfer with interfacial jump conditions, *Int. J. Heat Mass Transfer* **88**, 306 (2015).
- [14] C. Ferrari, B. Kaoui, V. S. L'vov, I. Procaccia, O. Rudenko, J. H. M. ten Thije Boonkkamp, and F. Toschi, Analytical modeling for the heat transfer in sheared flows of nanofluids, *Phys. Rev. E* **86**, 016302 (2012).
- [15] B. Kaoui, T. Krüger, and J. Harting, How does confinement affect the dynamics of viscous vesicles and red blood cells? *Soft Matter* **8**, 9246 (2012).
- [16] B. Kaoui, R. Jonk, and J. Harting, Interplay between microdynamics and macrorheology in vesicle suspensions, *Soft Matter* **10**, 4735 (2014).
- [17] J. Crank, *The Mathematics of Diffusion* (Oxford University Press, Oxford, 1975).